

# High-throughput Ultrasonic Implant Communication Link Using ML-assisted CDMA Decoder

*Sina Faraji Alamouti*



Electrical Engineering and Computer Sciences  
University of California, Berkeley

Technical Report No. UCB/EECS-2021-24

<http://www2.eecs.berkeley.edu/Pubs/TechRpts/2021/EECS-2021-24.html>

May 1, 2021

Copyright © 2021, by the author(s).  
All rights reserved.

Permission to make digital or hard copies of all or part of this work for personal or classroom use is granted without fee provided that copies are not made or distributed for profit or commercial advantage and that copies bear this notice and the full citation on the first page. To copy otherwise, to republish, to post on servers or to redistribute to lists, requires prior specific permission.

---

**High-throughput Ultrasonic Implant Communication Link Using ML-assisted CDMA Decoder**

by Sina Faraji Alamouti

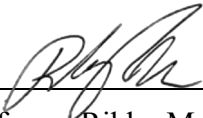
---

**Research Project**

Submitted to the Department of Electrical Engineering and Computer Sciences,  
University of California at Berkeley, in partial satisfaction of the requirements for the  
degree of **Master of Science, Plan II.**

Approval for the Report and Comprehensive Examination:

**Committee:**



---

Professor Rikky Muller  
Research Advisor

05/28/20

---

(Date)

\* \* \* \* \*



---

Professor Anant Sahai  
Second Reader

5/28/20

---

(Date)



# Acknowledgements

First, I would like to thank my advisor Prof. Muller for her guidance throughout this project that proved crucial to the successful demonstration of all achievements. I would also like to send special thanks to my colleague and my dear friend, Mohammad Meraj Ghanbari who was the critical element of this collaboration and whose diligence, creative mind, and passion made any progress in this project possible. This work was a collaboration at every single step and I hereby welcome Mr. Ghanbari to reuse or republish any or all of the details indicated here in the future dissertations. I would also like to express my gratitude towards the kind assistance of Prof. Anant Sahai for his guidance in choosing proper approaches when tackling the decoding problems as well as other colleagues, Nathan Tessema Ersumo, Alan Dong, and Nima Baniasadi who were of great help in various steps.

Finally, I'd like to thank my beloved family whose kind company I miss the most.

## Abstract

Development of prosthetic limbs that offer more degrees of freedom in gesture control can benefit from peripheral neural activity recording. A network of miniaturized wireless implants that sit locally near residual peripheral nerves in amputees and record and transmit high resolution neural activity can enhance the functionality of such prosthetics. Such a network can be realized using small ultrasonically operating motes and be interrogated with a single-element external transducer. Multiple access protocols are adopted to permit simultaneous communication with the individual motes.

This overall system is constrained not only by common issues associated with simultaneous multi-transmitter communication, but also by a set of requirements imposed due to the design of the ultrasonic motes, the power/data delivery protocols, the mechanical nature of ultrasonic transducers, as well as computational simplicity on the implant side. Achieving high throughput communication with the implants faces several challenges as a result.

This project aims to address those issues and offers a machine learning (ML) based approach that achieves near an order of magnitude of improvement in the bit-error rate (BER) performance compared to traditional methods. Compared to state-of-the-art, this work provides 4 times higher total channel capacity and the largest number of implants.

# Contents

Contents .....	3
List of Figures & Tables .....	4
1. Introduction .....	5
1.1. Motivation .....	5
1.2. System Overview .....	6
1.3. Measurement Setup .....	6
1.4. Focus of this thesis .....	7
2. Coding Scheme .....	8
3. Data Rate vs. Inter-symbol Interference (ISI) .....	11
4. ISI Mitigation .....	14
4.1. Min. Mean Squared Error (MMSE) equalization .....	14
4.2. Viterbi Trellis Decoder .....	16
5. Convolutional Neural Network based decoder .....	19
5.1. Data Preprocessing .....	19
5.2. Model Architecture .....	20
5.3. Evaluation Results .....	21
6. Comparison, Conclusion, and Future Work .....	23
Bibliography .....	25

# List of Figures & Tables

## Figures

1.1	Multi-site wireless peripheral neural recording concept .....	6
1.2	Measurement Setup .....	7
2.1	Sample OOK sequence .....	8
2.2	Encoder Schematic .....	9
2.3	The receiver chain structure .....	9
2.4	Despreading Governing Equations .....	10
3.1	ISI vs. number of cycles/bit .....	12
3.2	ISI in real packets .....	12
4.1	MMSE detector backend .....	15
4.2	MMSE detector BER vs Data rate .....	15
4.3	Channel memory and transitions .....	16
4.4	Viterbi Trellis Decoder State Diagram .....	17
4.5	Viterbi detector BER vs. Data rate .....	17
5.1	Data Pre-processing .....	20
5.2	CNN architecture .....	21
5.3	CNN-based detector BER vs. data rate .....	22
5.4	ML-assisted detector BER vs. SNR .....	22

## Tables

1.1	List of the configurations .....	10
1.2	Comparison with State-of-the-art .....	23



# Chapter 1

## Introduction

### 1.1 Motivation

Recording of residual peripheral neural activity from a large number of nerves has been shown to help with an enhanced control of prosthetic arms. In particular, chronic recording of such data provides higher degrees of freedom to mimic natural arm gestures [1], [2]. However, the prior art has mostly utilized a wired connection to a set of electrode arrays that prohibits the longevity of high-quality recordings. Furthermore, such a disruptive approach suffers from degradation of signal-to-noise (SNR) ratio due to the development of dead-zones around the electrode location [15]. As a result, a system consisting of miniaturized neural recording implants that can power up and communicate wirelessly are envisioned as a solution.

Figure 1 shows the concept of this solution with a handful of implants placed near the median and ulnar nerves. The system is comprised of a set of ultrasonically powered neural recording implants that are interrogated by an external transducer. Both digital and analog communication schemes have been investigated in several prior works. For instance, [11] shows both amplitude shift keying (ASK) and on-off keying (OOK) to establish data transmission for two motes. In addition, [4] has shown individual recording motes operating with an incoming ultrasound wave to send back recorded analog data using analog amplitude modulation (AM) backscattering. Further optimizations have been shown in [8] to linearly adjust the reflection coefficient of the ultrasonic transducer (in this case a piezo-electric device). Power-up and communication protocols have also been discussed in [3] to specify time windows available for uplink data transfer given a reasonable implantation depth of 50 mm. At such depths, ultrasound waves are preferred over radio frequency (RF) waves because of lower attenuation factor when propagating through the tissue [16] and hence are assumed as the carrier wave in this project. Despite covering a variety of multiplexing

schemes for the ultrasonic notes [6], no prior art to our knowledge has demonstrated simultaneous data recording from more than 2 implants. In this effort, the goal is to achieve a platform that can potentially accommodate simultaneous communication with 10s of ultrasonic implants. Required specifications and challenges associated with this target are elaborated on in the following sections and various solutions are discussed and evaluated in the later chapters.

## 1.2 System Overview

A network of ultrasonically powered implants can be placed near the residual peripheral nerves of severed limbs to monitor and record the neural activity. The implants can provide higher resolution information that will translate to more degrees of freedom in prosthetic limb control. High resolution recording of spiking neural data requires a minimum uplink data rate of  $\sim 200$  kbps (10 bits at  $\sim 20$  kS/s) per implant. In order to accommodate such data rates from 10s of different sites, a communication channel with  $>2$  Mbps capacity is required. Prior art in uplink communication of ultrasonic implants reports a maximum overall channel capacity of about 200 kbps [6], an order of magnitude lower than what the target application necessitates.

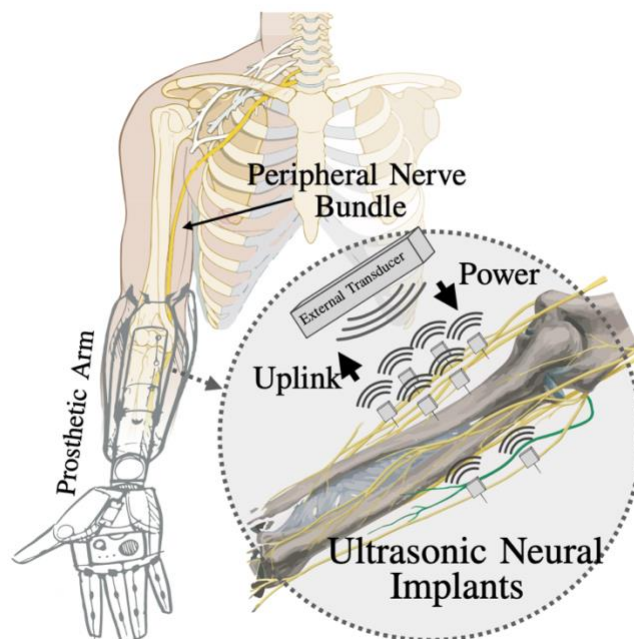


Figure 1.1 - Multi-site wireless peripheral neural recording concept. [3]

## 1.3 Measurement Setup

A setup consisting of 4 ultrasonic transducers over a printed circuit board (PCB) is made as shown in figure 1.2. These motes are driven using high-voltage driver boards (Maxim, MAX14808) that are controlled by an FPGA (Xilinx Spartan-6) controller. The received ultrasound signal is transduced into electrical voltage by an external probe. The induced voltage is then measured and digitized by an 8-bit Analog to Digital Converter (ADG9057). Finally, the PC receives the data through the FPGA interface allowing for all processing to happen in PC hardware. The propagation

medium is filled with Canola oil with similar acoustic properties to the tissue. Data packets are generated in PC, loaded onto FPGA and drive the Maxim boards to actuate the piezo transducers. The acoustic wave then travels through the medium, reaches the external probe and produces vibrations that cause an electric voltage. This voltage signal is eventually measured as ADC output. A set of 10,000 total packets for different configurations are collected to evaluate the performance of the communication link.

## 1.4 Focus of this thesis

The focus of this thesis is on the computing backend for the wireless receiver (Rx) implemented in the project. Several decoding schemes are discussed and implemented over MATLAB or Python environment. The Google TensorFlow library with Keras extension [7] is used to model the neural network. A performance comparison is made between the applied methods and finally a summary including a comparison with the best performing prior arts is presented.

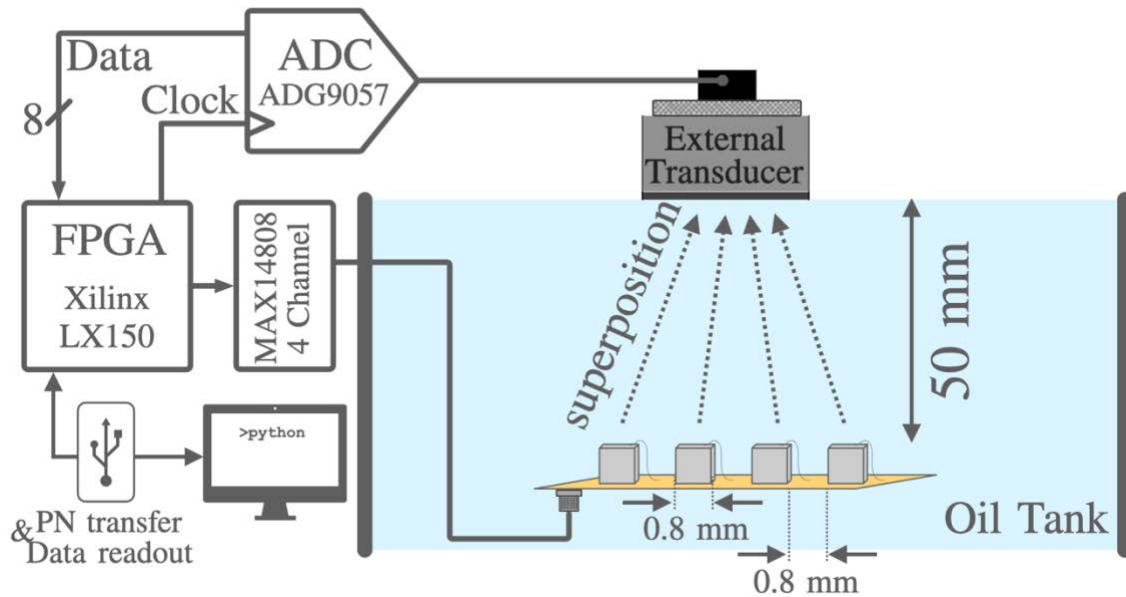


Figure 1.2 - Measurement setup [3]

## Chapter 2

# Coding Scheme

Analog code division multiplexing for the ultrasonic notes was shown for a set of two free-floating implants in [8]. The principle of operation was based on up-modulation of the analog recorded neural data by a sub-carrier frequency orthogonal to that of other implants and the external decoder took the charge of performing proper demodulation to extract the information. In this work, digital block-coded CDMA is employed that uses unique orthogonal codes per implant and the external unit retrieves the data after dispreading using the pre-assigned keys.

The modulation scheme used on the implants side is a simple amplitude on-off keying (OOK) through which the implants either send a maximum amplitude pulse or a zero signal. This can be viewed in figure (2.1) as a bit stream of “10101” is sent.

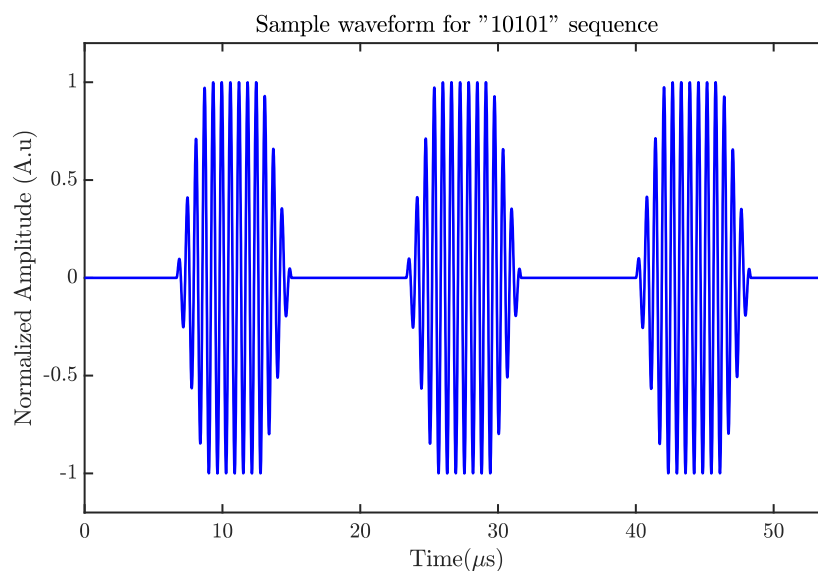


Figure 2.1 - Sample OOK Sequence

Here, since the data rate requirements are already stringent, no redundancy in the code structures are considered. Since there are 4 individual motes in the setup, the codes are taken from rows of a 4x4 Walsh-Hadamard matrix as shown below.

$$H_b(2^2) = \begin{bmatrix} 0 & 0 & 0 & 0 \\ 0 & 1 & 0 & 1 \\ 0 & 0 & 1 & 1 \\ 0 & 1 & 1 & 0 \end{bmatrix}$$

If the codes are taken from a 4x4 identity matrix (I), the resulting coding structure would belong to Time-Division Multiplexing (TDM). This shows that CDMA has the penalty of higher power level (more energy in a single time frame) and the overlap of levels from different transmitters to achieve a more robust communication in presence of multipath reflection. Figure 2.2 shows the structure of encoder on the implant side. The bits of information are XORed with the key and the final stream is applied to the OOK transmitter driver. Eventually at the receiver end, the waves from all implants are superimposed in the acoustic domain and form a multi-level signal that follows the direct summation of the codes.

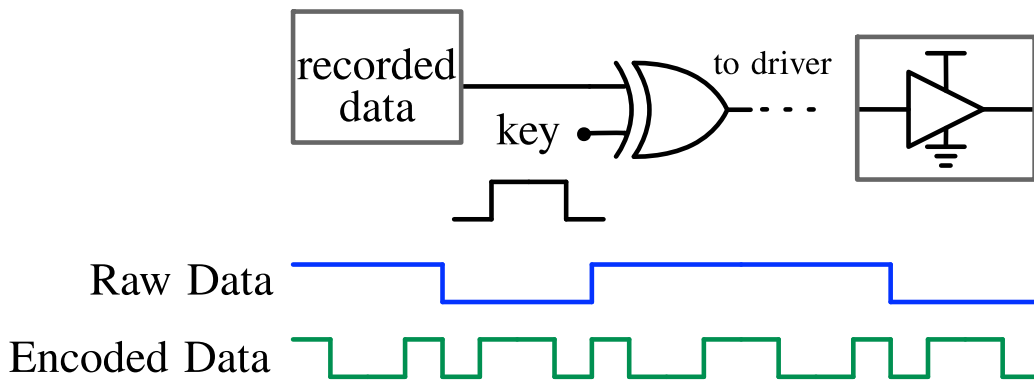


Figure 2.2 - Encoder Schematic

On the receiver end, the backend is comprised of a detector that decodes the received waveform and outputs a CDM sequence which is then used to extract individual bits of information. Shown in figure 2.3 is the structure of the receive chain. A despreading block applies the CDM key of each implant to the detected sequence to remove the data content of other motes, leaving only the transmitted bit of that particular implants.

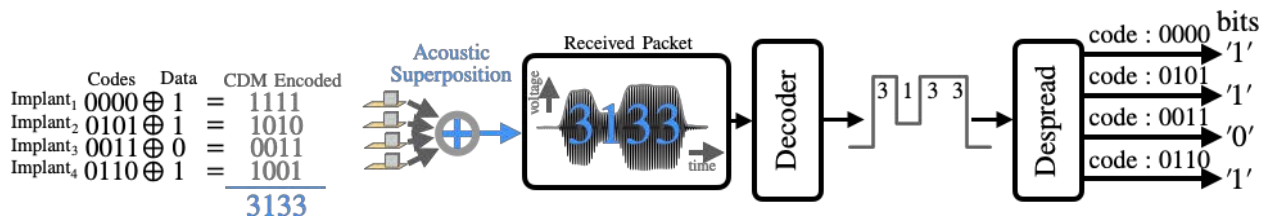


Figure 2.3 - The receiver chain structure

In order to despread the received sequence, a simple one-to-one mapping is applied to convert the received sequence into a DC-balanced version and then the resulting sequence is multiplied by the DC-balanced pre-assigned keys. The outgoing sequence is then integrated over the symbol duration and the sign of integration output determines the actual bit of information. Figure 2.3 shows such steps for a sample received waveform. Table 2.1 lists all of the configurations implemented in this project. This includes a range of different data rates, based on different number of symbols per packet of transmission or the allocated number of ultrasound cycles per bit of transfer.

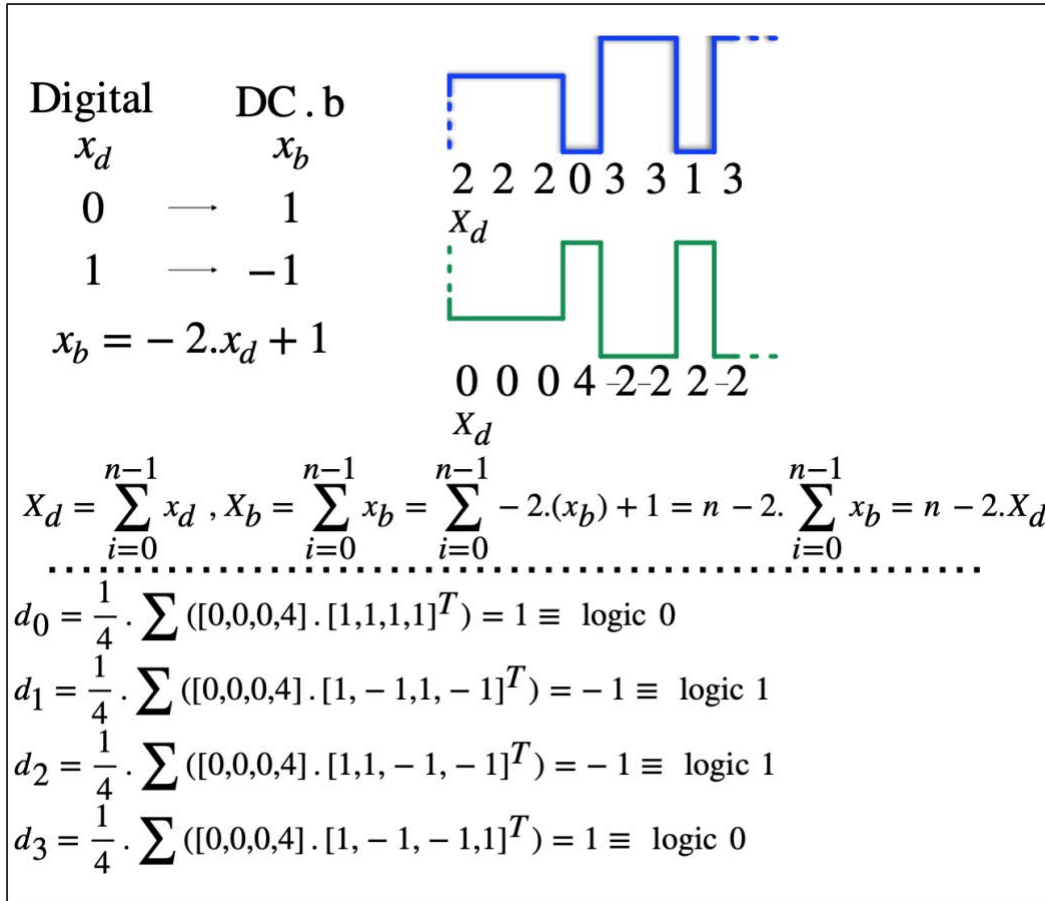


Figure 2.3 - Despreading Governing Equations

Config #	0	1	2	3	4	5	6
# Symbols/packet	14	12	7	6	4	2	1
Carrier Cycles/Bit	1	1	2	2	3	7	14
Data Rate [kbps]	784	672	392	336	224	112	56

Table 2.1 - List of the configurations

## Chapter 3

# Data Rate vs. Intersymbol Interference (ISI)

In the previous chapter, we discussed that the ultrasound transducers are used as antennas for signal transmission. Such devices can be made of piezoelectric materials that vibrate in response to the applied electrical voltage signal and produce the acoustic waves. On the other hand, they can be actuated acoustically as well to reproduce an electric signal across their terminals. Due to the mechanical nature of the vibrations, these transducers suffer from a limited mechanical bandwidth (BW) and as a result cannot allow rapid deformations when receiving rapid voltage actuations.

As mentioned in the previous chapter, the modulation scheme used here is a simple OOK which allows for only two amplitude levels of transmission. As a result, the only way to increase the transmission data rate is to include more and more bits into the same number of cycles, thereby increasing the bit/cycle ratio. At the maximum possible limit, there is only 1 ultrasound cycle for 1 bit of information for each mote. However, in reality a single cycle drive of piezo device produces multiple cycles of ultrasound waves due to the mechanical ringing in response to the applied actuation. Figure 3.1 depicts the resulting waveform for a 3-bit drive of implant transducers when the number of cycles per bit is reduced.

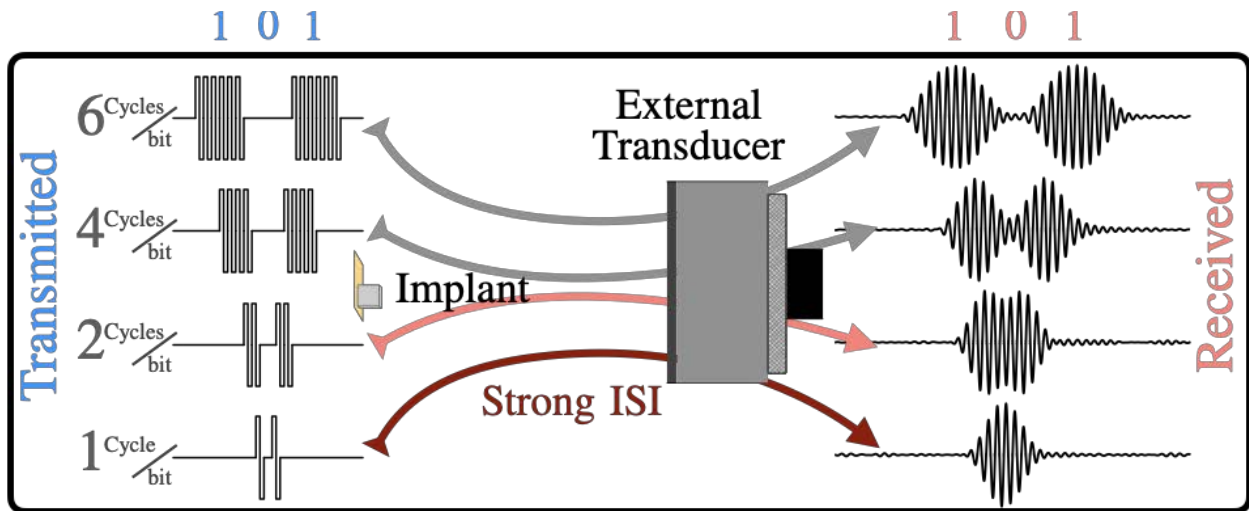


Figure 3.1 - ISI vs. number of cycles/bit

As can be seen from figure 3.1, for higher data rates, consecutive bits merge together. This causes an extremely strong intersymbol interference (ISI) that prohibits easy detection of multi-bit symbols. As discussed in the previous chapter, the configurations for different data-rates include symbols of 4 bits, each 1 to 14 ultrasound cycles long, resulting in 56 kbps to 784 kbps data rates respectively. The ultrasound waves transmitted from individual implants propagate toward the external transducer and the receiver gets a summation of those incoming waves. Figure 3.2 compares two samples of such overall waveforms as plotted with respect to time for two different configurations.

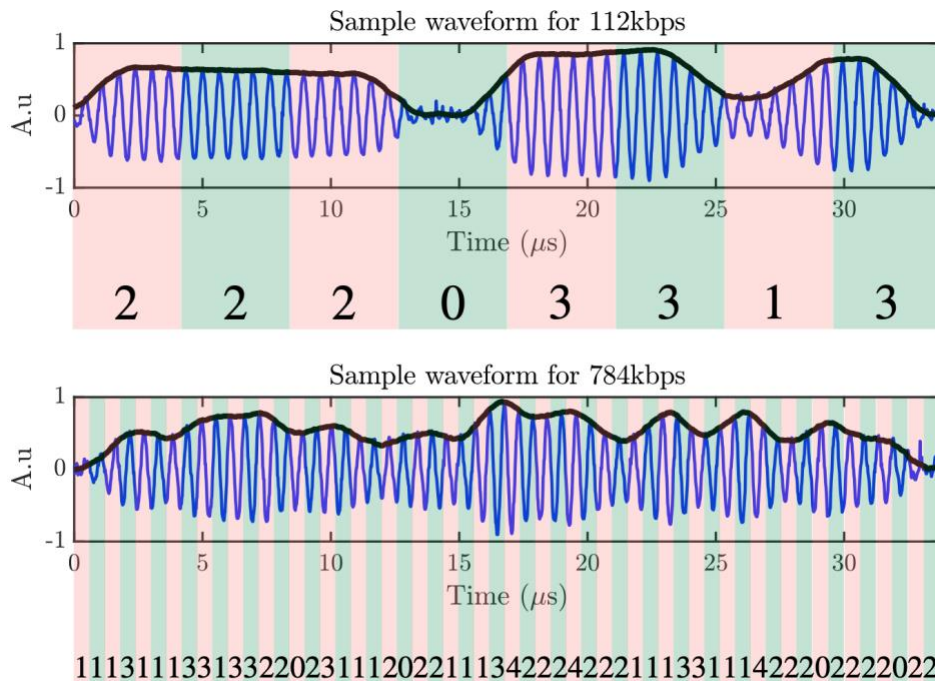


Figure 3.2 - ISI in real packets.



As shown in the figure, at higher data rates, none of the symbols can be clearly distinguished and all transitions are dissolved into the neighboring levels. This makes the job of the detector extremely difficult to retrieve the correct sequence. Hence, a set of different approaches are implemented as discussed in the next chapter to mitigate this ISI effect and detect the received packets in all configurations.

# Chapter 4

## ISI Mitigation

The literature of digital communication systems covers a deep variety of pre- and post-transmission techniques to enhance the performance of the communication link against ISI. This includes but is not limited to error minimization methods based on certain criteria (such as Mean Squared Error etc.) as well as maximum likelihood detectors that pick the most probable sequence when receiving a certain waveform. Here, due to computational complexity as well as tight requirements on the overall channel capacity, only two of the most common methods are practiced, namely, a Minimum Mean Squared Error (MMSE) detector [17] as well as a Maximum Likelihood Viterbi Trellis decoder [18]. Section 4.1 expands on the implementation of MMSE algorithm and discusses its limitation. In section 4.2, the trellis decoder is introduced and evaluated for the system. Finally, section 4.3 elaborates on the shortcomings of each method and provides an insight on how to take advantage of a smarter decoder in later chapters.

### 4.1 MMSE Detector

The idea behind an MMSE detector is to learn the effect of channel using a set of pre-known pilot signals and then try to revert that effect by means of training a set of equalization weights. This approach excels in moderate ISI conditions and delivers a suitable performance at a very insignificant computation cost. Depending on how fast the channel parameters change, updates will be necessary to the equalizer weights which requires retransmission of pilot signals. This introduces a data rate overhead that can be costly at fast-changing channel conditions. There exist other similar approaches that do not require constant updates to the channel state information (CSI), and instead rely on a predicted joint distribution for those parameters. These decoders, known as “Blind MMSE Detectors”, work at the expense of higher error probability and as a result are not ideal for bit error rate (BER) sensitive applications. The backend core for MMSE equalization is implemented in MATLAB software. The block diagram of the system is shown in figure 4.1.

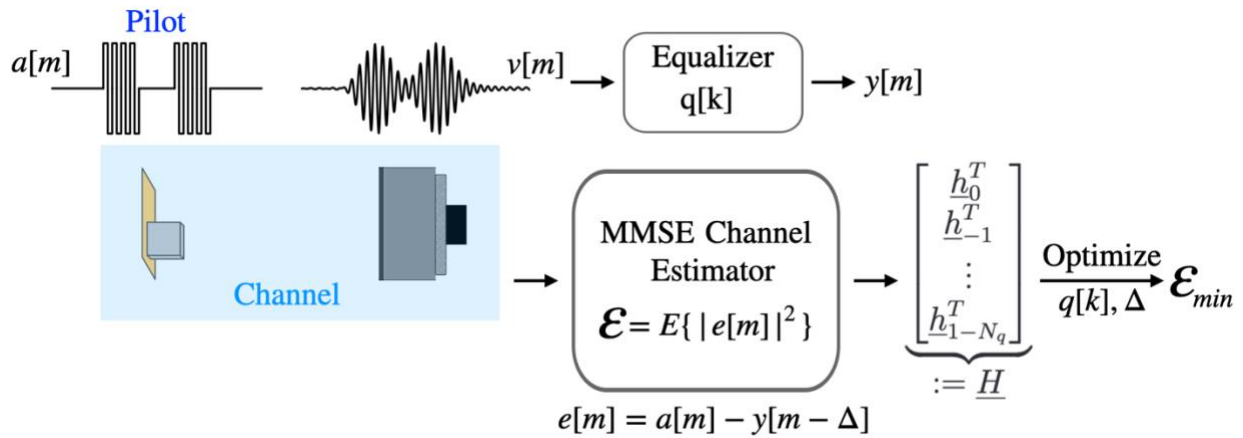


Figure 4.1 - MMSE Detector Backend

The equalizer weights are fit based on a set of training samples consisting of 4,000 packets for each configuration. The resulting equalizer is then used to decode the remaining test waveforms and the detection error is evaluated at each configuration. Figure 4.2 plots the achieved BER vs. the data-rate of transmission. As seen in figure 4.2, at lower data rates, the detector performs well in decoding the received sequences and remains error free up to 1E5 tested bits. However, at even a moderate data rate of 224 kbps, the BER rises to 2E-3 which is a considerable change. It further degrades at higher data rates, essentially making a reliable communication at those configurations infeasible.

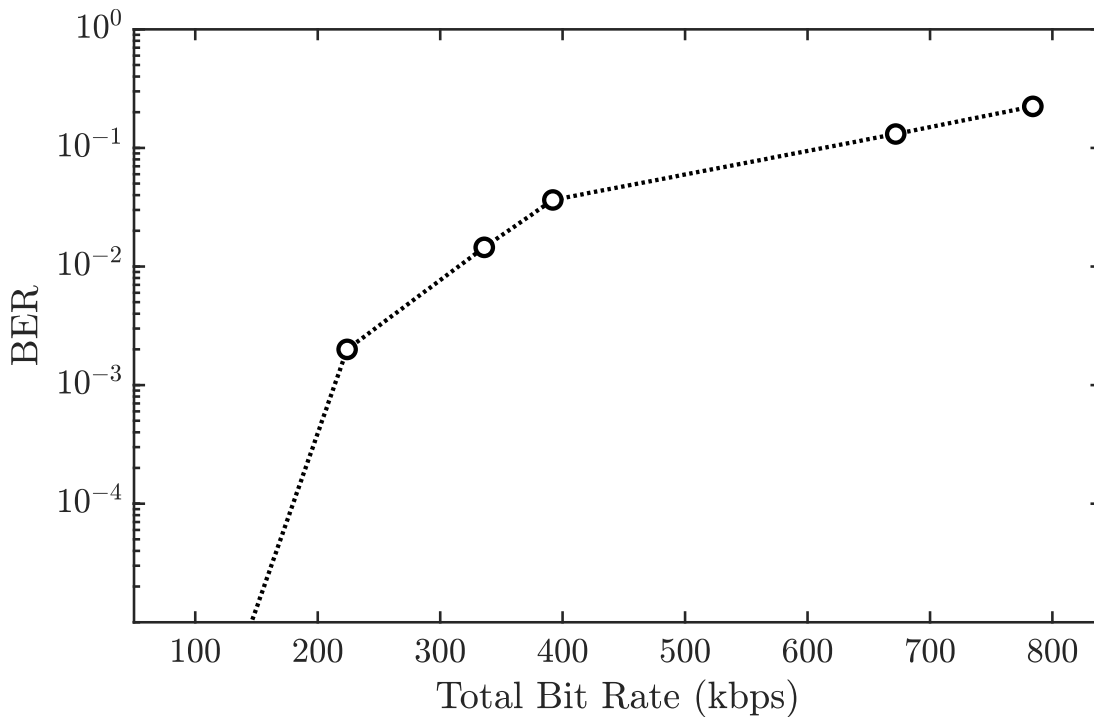


Figure 4.2 - MMSE detector BER vs Data Rate

## 4.2 Viterbi Trellis Decoder

As seen in the previous section, the MMSE decoder was unable to deliver the needed performance at higher data rates. This is mainly due to the strong ISI and the fact that a set of linear weights cannot provide an accurate mapping for the superposition of tightly sitting symbols produced from the input patterns. In this section, inspired by the Viterbi Maximum-Likelihood decoder for convolutional source encoding schemes, a trellis is introduced that consists of a set of states that represent the previously transmitted symbols, and this way in effect, the memory of the channel is reconstructed and certain patterns are learnt to help detect the correct sequence.

First, the memory length of the channel is evaluated. This can be approximated by monitoring a single “1” to “0” or “0” to “1” transition. Looking at figure 4.3 from the actual measurements, it can be seen that the transient response dies out after about 6 ultrasound cycles.

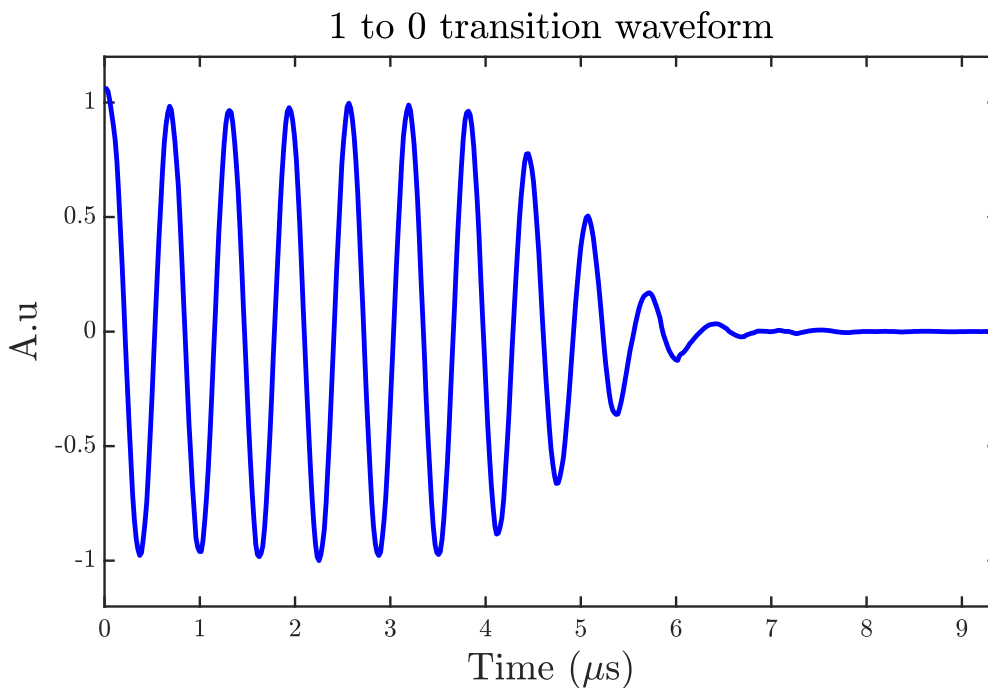


Figure 4.3 - Channel memory and transitions

As a result, a detector that monitors the current symbol while considering the previous six-cycle window can find the sequence with highest correlation to the received waveform. In this work, a decoder backend is coded in MATLAB that starts from the first symbol and adds every symbol that is decoded into the decoder state. Figure 4.4 shows a block diagram of the detector with two symbols memory.

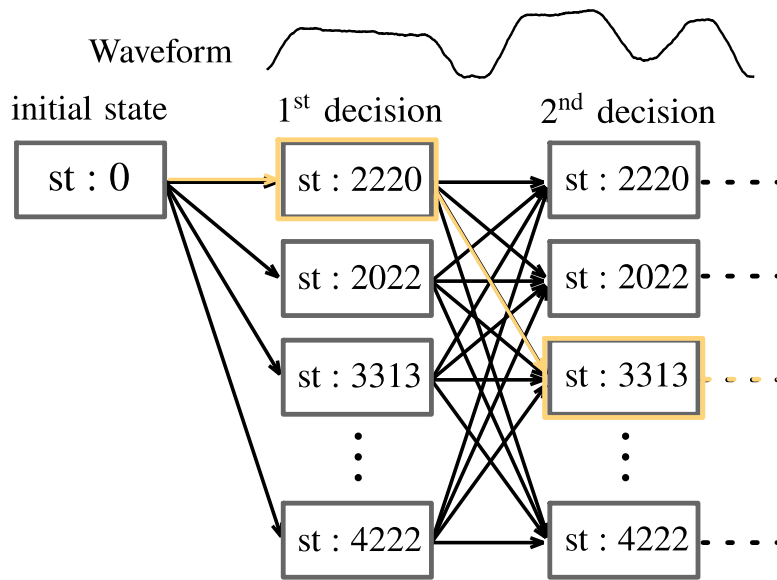


Figure 4.4 - Viterbi Trellis Decoder State Diagram

The new decoder is also evaluated using the same training and test datasets. Figure 4.5 shows the plot of BER vs. Bit rate for this detector. In comparison with the MMSE decoder, up to 200× of improvement in BER is achieved in certain configurations when the Viterbi trellis decoder is employed.

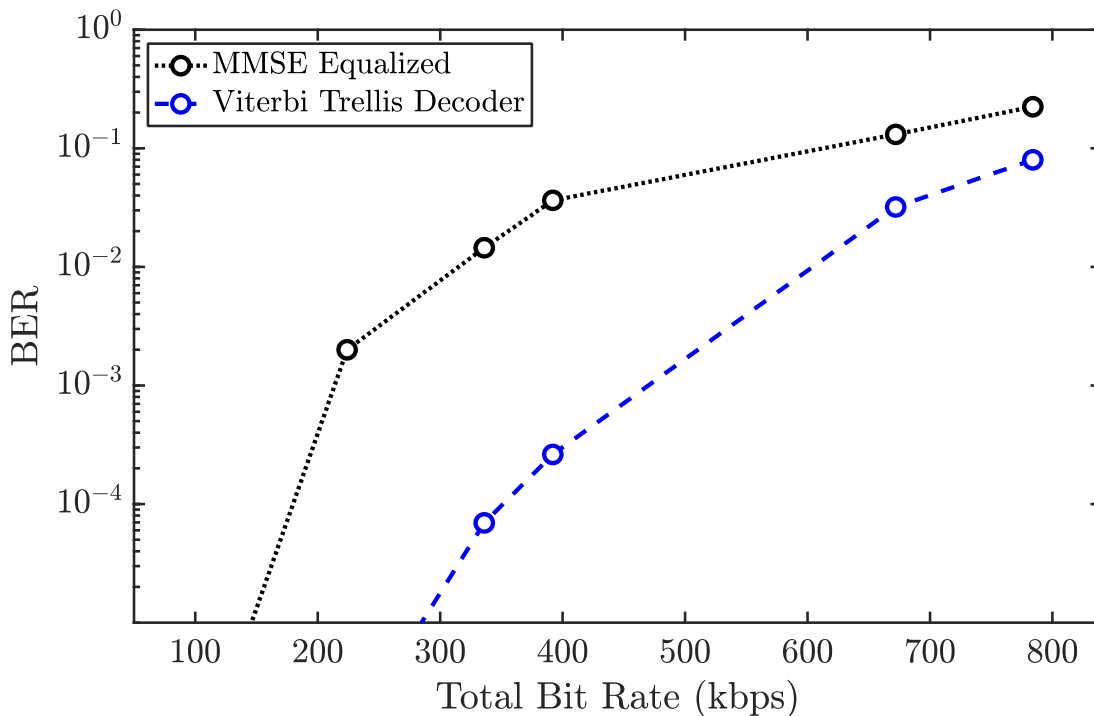


Figure 4.5 - Viterbi Decoder BER vs. Data rate

The experiments with MMSE and Viterbi decoders demonstrated that at higher ISI conditions, a detector that evaluates the set of symbols together and decodes the received packet as a whole can outperform the ones with narrower decoding window. This encourages an attempt to develop a decoder that detects the entire sequence all at once. This is in essence very similar to an optimal decoder which finds the pattern with the highest cross-correlation between all possible patterns. The computational complexity of the optimal decoder prohibits its application for high data rate configurations simply because of vastly large number of possible patterns. On the other hand, if a decoder is trained to learn the entire packet as a whole rather than constantly computing cross-correlation, a superior performance can be obtained. This raises the idea of employing a class of machine learning models that excel at interpretation and classification of images, namely, Convolutional Neural Networks (CNN). The next chapter goes over the CNN model that is used as a decoder to achieve a much more desirable BER performance.

## Chapter 5

# Convolutional Neural Network (CNN) based decoder

In the previous chapter, the shortcomings of MMSE and Viterbi decoders were discussed. The motivation behind developing a neural network (NN) model is the fact that raw data can be input to the model with no manual feature extraction and the entire sequence will be observed as a whole. The application of ML based decoders has long been discussed in the literature. Azhang *et al.* [9] demonstrated a NN based approach that could outperform the traditional matched filter implementations and deliver near optimal performance. Farsad *et al.* [10] also discusses how a bidirectional recurrent neural network (BRNN) can excel at continuous multi-symbol detection of transmitted signals impacted by strong ISI.

Here, a CNN based model is designed to benefit from the parameter sharing of the kernels, thereby reducing the number of model parameters. Few pre-processing steps are taken to scale the voltage waveforms into images that can be properly fed to the model. Section 5.1 reviews all the pre-processing steps and determines the size of the model input layer. The architecture of the model is shown and discussed in section 5.2, and finally the results using this decoder are provided in section 5.3.

### 5.1 Data Preprocessing

Figure 5.1 depicts a sample waveform received at the output of the transceiver. In order to prepare the input 1-dimensional images for the model, the envelope of the samples is first extracted. The waveforms are then passed through a standard scaling process to normalize the amplitude into  $[0,1]$  range. The final output image is shown in Figure 5.1 as well. In our system, the normalized input images are at maximum 1750 pixels wide which is a reasonable length for the model. In case of extended images in future experiments, it is possible to downsample the extracted envelope to reduce the number of sample points, and the image size as a result.

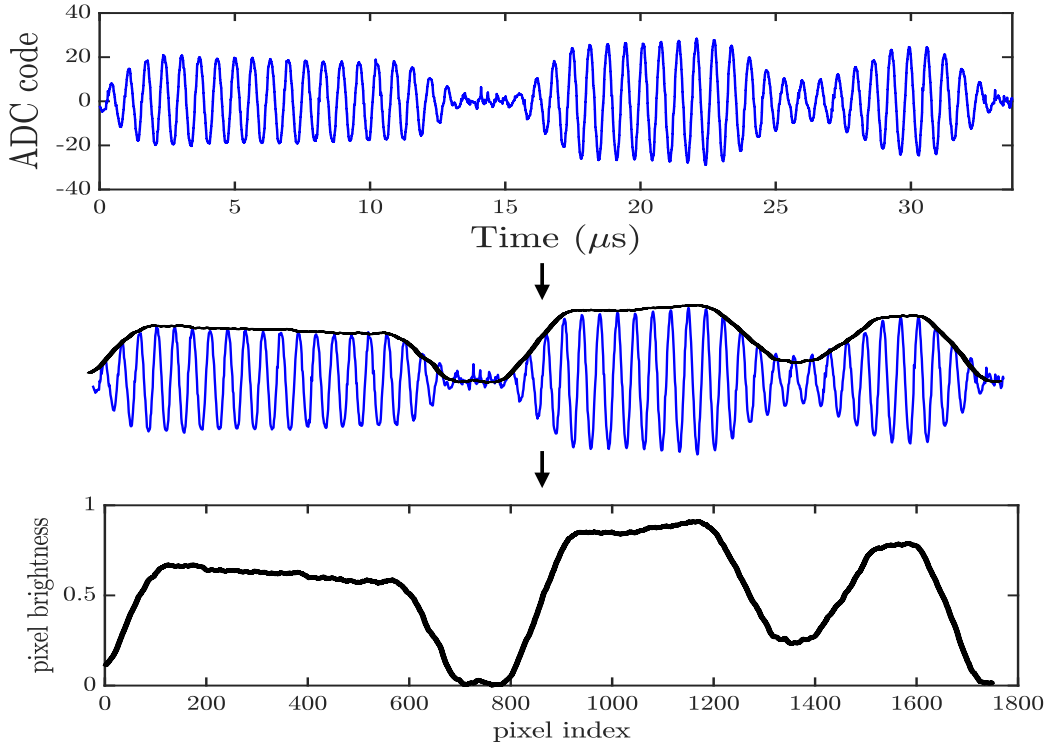


Figure 5.1 - Data Pre-processing

Finally, the samples are divided into three sets for training, validation, and testing of model. Out of 10,000 recorded packets, 4,000 samples are used for the training phase, 1000 are assigned for validation to tune the hyper parameters, and the remaining 5,000 packets form the test dataset. For the last two configurations that have a higher data-rate, this ratio changes to include 6,400 samples for the training phase. This allows a better performance as in those cases the input data has a much higher degree of freedom and variability.

## 5.2 Model Architecture

The CNN architecture is shown in Figure 5.2. The number of hidden layers, the kernel sizes, as well as the size of the final fully connected (FC) layer is determined by monitoring the training and validation losses and accuracies. The model is defined as a regressor that outputs the detected value for each level through the output sequence. Using one-dimensional kernels, larger kernel sizes can be selected that cover a wider section of the input image at each cross-correlation operation, allowing for more long-lasting features to be perceived. Finally, a dropout layer with a ratio of 0.1 is applied before the last layer to reduce the model overfitting. The model is then compiled with “mean squared error” (MSE) loss function and “Adam” optimizer is used with a learning rate of 0.01. Batches of 50 samples are used to speed up the training phase and each model for each configuration is trained for 50 epochs. Next section will discuss the evaluation results in detail.



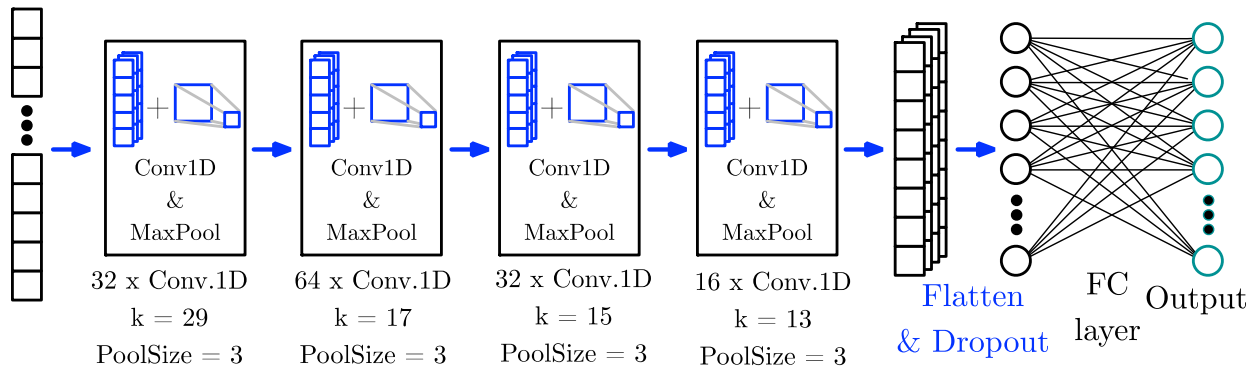


Figure 5.2 - CNN architecture

### 5.3 Evaluation Results

The CNN model is trained at each different configuration. Figure 5.3 plots the achieved BER at different configuration. As seen in the plot, using the CNN-based decoder, the BER at the highest data rates is kept below  $1E-3$  limit which allows a reliable communication for the target application. As seen in the plot, at data rates lower than 672 kbps, the transmission happens error free for up to  $1E5$  bits. This significantly improves the BER compared to the previous detectors.

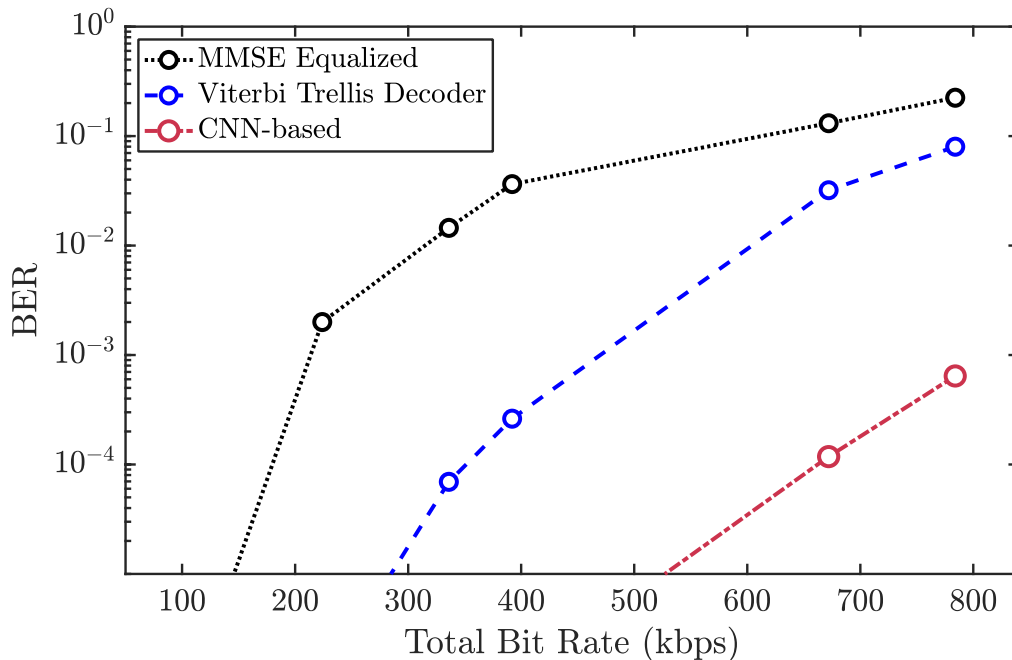


Figure 5.3 - CNN-based detector BER vs. data rate

## Effect of Signal-to-Noise Ratio (SNR)

The SNR of the collected data in the setup is about 35 dB. All of the previous experiments were done with data with this SNR level. In this section, in order to evaluate the performance of the model in different SNR levels, in-band Gaussian noise computationally is added to the collected samples to give an SNR range of 0 dB to 35 dB. The model is then retrained and retested using noisy samples and the results are shown in Figure 5.4. As expected, the number of error bits increases as the noise level goes up. Even at a reasonable SNR level of 25 dB, data rates as high as 392 kbps can be achieved with a BER less than  $1E-3$ .

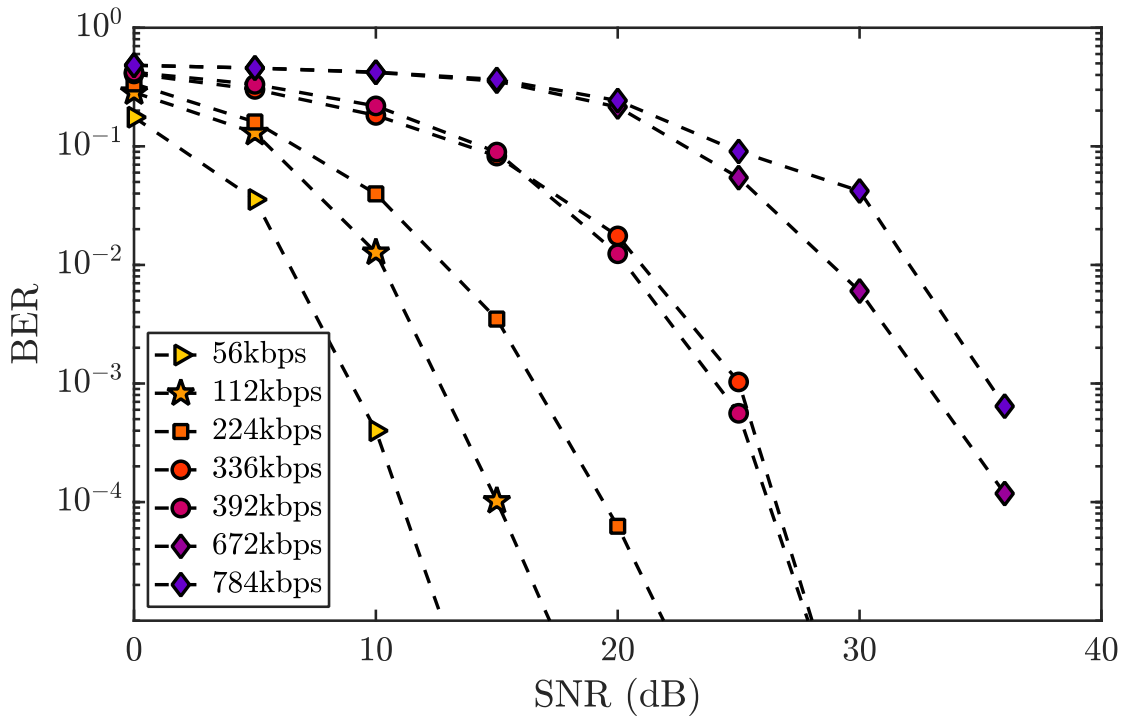


Figure 5.4 - ML-assisted detector BER vs. SNR

## Chapter 6

# Comparison, Conclusion, and Future work

In this chapter, the state of the art for uplink communication link in the ultrasonically powered implants are reviewed. Table 6.1 lists the important specifications for the selected prior arts compared to this work. This work doubles the number of measured implants over prior art. The total channel capacity is improved by a factor of 4, and the spectral efficiency (SE) is 6.3 times better than the best prior art. Furthermore, this work only utilizes a single external transducer that facilitates the alignment of transducer elements and reduces the cost of the entire setup.

	[11]	[12]	[13]	[14]	[6]	<b>This work</b>	<b>This work</b>	<b>This work</b>
No. of Implants	2	1	1	1	2	<b>4</b>	<b>4</b>	<b>4</b>
Piezos per Implant	1	2	1	2	2	<b>1</b>	<b>1</b>	<b>1</b>
External Elements	32	2	2	2	32	<b>1</b>	<b>1</b>	<b>1</b>
Depth [mm]	60	85	120	37.5	65	<b>50</b>	<b>50</b>	<b>50</b>
$f_c$ [MHz]	1	2.5	0.79	1	2.52	<b>1.6</b>	<b>1.6</b>	<b>1.6</b>
Uplink [kbps]	50	100	10	75	194	<b>392</b>	<b>672</b>	<b>784</b>
SE* [kbps/MHz]	50	40	12.6	75	77	<b>245</b>	<b>420</b>	<b>490</b>
BER	–	1E-4	1E-5	–	1E-4	<b>1E-5</b>	<b>1.2E-4</b>	<b>6.4E-4</b>

\* Spectral Efficiency

Table 6.1 - Comparison with State-of-the-art

In conclusion, an uplink ultrasound communication channel consisting of 4 ultrasonic implants is presented. Using a novel CNN-based decoder, the BER performance of the link is enhanced by almost 3 orders of magnitude compared to conventional MMSE detectors. This work

advances the state of the art in both total channel capacity as well as number of implants and provides a promising vision to achieve a robust communication for multi-implant neural recording networks.

Looking forward, the carrier frequency of the piezoelectric transducers can scale to 5 MHz, potentially allowing a total uplink capacity of 2.44 Mbps, which meets the demand of the target application. Further techniques in the source and channel coding can be employed to enhance the performance at lower SNR levels. In addition, the performance of model should be evaluated under changing channel conditions and potential online learning capabilities should be investigated to track varying features.

# Bibliography

- [1] – G.S. Dhillon *et al.*, “Residual Function in peripheral nerve stumps of amputees: implications for neural control of artificial limbs,” *The Journal of hand surgery*, vol. 29, no. 4, pp. 605-615, 2004.
- [2] – P.M. Rossini *et al.* “Double nerve intraneural interface implant on a human amputee for robotic hand control,” *Clinical neurophysiology*, vol. 121, no. 5, pp. 777-783, 2010.
- [3] – S.F. Alamouti\*, M.M. Ghanbari\*, *et al.* “High Throughput Ultrasonic Multi-implant Readout Using a Machine-Learning Assisted CDMA Receiver,” In *2020 42nd Annual International Conference of the IEEE Engineering in Medicine and Biology Society (EMBC)*. IEEE, 2020.
- [4] – M.M. Ghanbari, *et al.* “17.5 a 0.8 mm 3 ultrasonic implantable wireless neural recording system with linear am backscattering,” In *2019 IEEE International Solid-State Circuits Conference-(ISSCC)*. IEEE, 2019, pp. 284-286.
- [5] – DJ. Seo *et al.* “Neural Dust: An Ultrasonic, Low Power Solution for Chronic Brain-Machine Interfaces”. In: arXiv (July 2013).
- [6] – T.C. Chang, *et al.* “Multi-access networking with wireless ultrasound-powered implants,” *2019 IEEE Biomedical Circuits and Systems Conference (BioCAS)*. IEEE, 2019, pp. 1-4.
- [7] – Martín Abadi, *et al.* “TensorFlow: Large-scale Machine Learning on Heterogenous Systems,” *2015*, Software available from tensorflow.org.
- [8] – M.M. Ghanbari, *et al.* “A sub-mm 3 ultrasonic free-floating implant for multi-mote neural recording,” *IEEE Journal of Solid-State Circuits (JSSC)*, vol. 54, no. 11, pp. 3017-3030, 2019.
- [9] – B. Azhang, *et al.* “Neural Networks for multiuser detection in code-division multiple-access communications,” *IEEE Transactions on Communications*, vol. 40, no. 7, pp. 1212-1222, 1992.

- [10] – N. Farsad *et al.* “Neural Network detection of data sequences in communication systems”, *IEEE Transactions on Signal Processing*, vol. 66, no. 21, pp. 5663-5678, 2018.
- [11] – M.L . Wang *et al.*, “Closed-loop ultrasonic power and communication with multiple miniaturized active implantable medical devices,” in *2017 IEEE International Ultrasonics Symposium*, 2017, pp. 1–4.
- [12] – T. C. Chang *et al.*, “27.7 a 30.5 mm 3 fully packaged implantable device with duplex ultrasonic data and power links achieving 95kb/s with  $<10^{-4}$  ber at 8.5 cm depth,” in *2017 IEEE International Solid- State Circuits Conference (ISSCC)*. IEEE, 2017, pp. 460–461.
- [13] – M. Weber *et al.* “A miniaturized single-transducer implantable pressure sensor with time-multiplexed ultrasonic data and power links,” *Journal of Solid-State Circuits*, vol. 53, no. 4, pp. 1089–1101, 2018.
- [14] – M. Meng, *et al.* “Gastric seed: Toward distributed ultrasonically interrogated millimeter-sized implants for large-scale gastric electrical- wave recording,” *IEEE Transactions on Circuits and Systems II: Express Briefs*, vol. 66, no. 5, pp. 783–787, 2019.
- [15] – F. Pothof, *et al.* “Comparison of the in-vivo neural recording quality of floating and skull-fixed silicon probes,” in *2017 8th International IEEE/EMBS Conference on Neural Engineering*, 2017, pp. 158–161.
- [16] – Hoskins PR, Martin K, Thrush A, editors (2010) *Diagnostic Ultrasound: Physics and Equipment*. New York: Cambridge University Press.
- [17] – U. Madhow, *et al.* “MMSE interference suppression for direct-sequence spread-spectrum CDMA,” *IEEE transactions on communications* 42.12 (1994): 3178-3188.
- [18] - G. D. Forney, “The viterbi algorithm,” *Proceedings of the IEEE*, vol. 61, no. 3, pp. 268–278, March 1973.